Remote Sensing Applications: Society and Environment 32 (2023) 101072

Contents lists available at ScienceDirect

Remote Sensing Applications: Society and Environment

journal homepage: www.elsevier.com/locate/rsase

Large-scale water balance modeling using remote sensing and weather data: Application in an agricultural growing region of the coastal northeast Brazil

Franzone Farias [a, *], Antônio Teixeira [a], Inajá Sousa [a], Janice Leivas [b], Celina Takemura [b], Edlene Garçon [b]

[a] Federal University of Sergipe (UFS), São Cristóvão, SE, Brazil
[b] Embrapa Territory, Campinas, SP, Brazil

ARTICLE INFO

Keywords:
Precipitation
Evapotranspiration
Water resources
SAFER
SEALBA

ABSTRACT

The SAFER (Simple Algorithm for Evapotranspiration Retrieving) algorithm was applied to test water balance (WB) monitoring in the agricultural growing region of SEALBA, an acronym for the states Sergipe (SE), Alagoas (AL), and Bahia (BA), coastal Northeast Brazil, classifying the biomes Atlantic Forest and Caatinga. The MODIS MOD13Q1 reflectance product and meteorological data were used to calculate actual (ET) and reference (ET_0) evapotranspiration at 16-day timescale along the years 2007–2021. The period with the highest precipitation (P) is in May, when the 16-day values are above 90 mm in Atlantic Forest and higher than 70 mm in Caatinga. For ET, the largest rates occur between July and September, when the 16-day average surpass 2.70 mm d^{-1} in the Atlantic Forest and 2.90 mm d^{-1} in Caatinga. Larger P together with lower ET, concentrates the positive water balance - WB (P – ET) from March to August in both biomes, bringing suitability for the rainfed agriculture. However, from July to December occur the negative WB values, indicating the need of irrigation for critical crop stages. Inferring the root-zone moisture conditions throughout the evaporative fraction values ($ET_f = ET/ET_0$) it is noticed that their highest values occur from April to October, evidencing a delay between the moment in which rainfall attend evapotranspiration with that in which the root-zone moisture recovers the optimum levels after the driest periods, what was also confirmed by the Pearson correlation coefficient values. The large-scale modelling carried out in SEALBA, presented viability to subsidize public policies regarding the water resources, with potential for replication of the methods in other regions.

1. Introduction

Observations and modellings have been demonstrated evidence of changes in the climatic systems worldwide, which are connected to human activities (IPCC et al., 2023). In addition to these climate changes, the expansion of agriculture over the natural ecosystems has caused large alterations in the river flows and ground tables, what can, with bad agricultural managements, contribute to environmental degradation, affecting the water fluxes between the surfaces and the low atmosphere and water qualities (Akhtar et al., 2021; Oliveira-Júnior et al., 2022; Silva et al., 2023). Considering these scenarios, the use of remote sensing with satel-

* Corresponding author.
E-mail addresses: franzone.farias@hotmail.com (F. Farias), heribertoteixeira11@gmail.com (A. Teixeira), inajafrancisco@gmail.com (I. Sousa), janice.leivas@embrapa.br (J. Leivas), celina.takemura@embrapa.br (C. Takemura), edlene.garcon@embrapa.br (E. Garçon).

https://doi.org/10.1016/j.rsase.2023.101072
Received 23 February 2023; Received in revised form 19 September 2023; Accepted 26 September 2023
Available online 11 October 2023

lite images together with meteorological data is highlighted for monitoring these impacts when aiming a sustainable development (Teixeira et al., 2020; 2021; Jardim et al., 2022).

Climate, land use, and land cover (LULC) changes has affected the water balance in several hydrological basins bringing importance of accounting the component of this balance for rational water resources managements (Yang et al., 2016; Zhang and Zhang, 2019). The Brazilian biomes Atlantic Forest (AF) and Caatinga (CT) inside the agricultural growing region in the coast of Northeast Brazil (NEB), limited by the states of Sergipe (SE), Alagoas (AL), and Bahia (BA), called SEALBA, for example, are suffering several impacts upon these resources, as consequence of deforestations, burnings, water pollution, and intensive agriculture, demanding large-scale water balance studies to support the sustainable consumptions of the water resources (Leivas et al., 2017; Araujo et al., 2019; Santos et al., 2020; Teixeira et al., 2021; Jardim et al., 2022; Oliveira-Júnior et al., 2022; Silva et al., 2023).

Local measurements of the water balance components are not suitable for large-scale analyses, due to variations on the environmental conditions, mainly under climate and land use changes scenarios. Because of these limitations, remote sensing from satellites together with geographic information systems have been used for these analyses through algorithm applications in distinct agroecosystems (Kamble et al., 2013; Wagle et al., 2017; Nyolei et al., 2019; Santos et al., 2020; Teixeira et al., 2021; Silva et al., 2023). These algorithms are very useful for quantifying the impacts from human activities upon natural resources (Sandre Osorio and Murilo, 2008), due to the efficiencies for quantification of water and vegetation parameters at different spatial and temporal resolutions (Asokan et al., 2020). The variables which affect the soil moisture levels in the root-zones are precipitation, irrigation, surface runoff, deep percolation, capillarity rise, evapotranspiration, and the change in soil water storage (Raes et al., 2009). Although evapotranspiration is related to crop production, increases on its rates mean lower water availability for ecological and human consumptions.

Crop production under the environmental conditions of SEALBA has gained room in economy over the last years. In the portion much closer to the coastline, predominate the AF biome and more to the west side is the CT biome. In both biomes, climate and land use changes are occurring. The AF has humid tropical climate, but its microclimates are contrasting mixtures of natural vegetation and anthropized areas (Ribeiro et al., 2009) while the species from Caatinga suffer of more drought periods along the year, developing resilience with the aridity increases (Jardim et al., 2022). Despite their suitability of the climate for agriculture, the fast replacement of the natural ecosystems, coupled with climate changes, have been contributing to the environmental instabilities, worsening the water resources competitions among distinct water users (Teixeira et al., 2020).

The delimitation of the agricultural potential for SEALBA was based on the average precipitation range from 450 to 1400 mm, from April to September. According to Procópio et al. (2019), this precipitation range could supply water for several grain crops (corn, bean, sorghum, rice etc.), with potential for rational expansion of other crops. However, to know the real water availabilities for agriculture, besides precipitation as input of water, the output, represented by evapotranspiration, must be also accounted (Filho et al., 2021). Some local water balance studies were carried out throughout local measurements in the biomes Atlantic Forest (Pereira et al., 2010; Rodrigues et al., 2021) and Caatinga (Silva et al., 2017; Marques et al., 2020), but few efforts have been done with the use of remote sensing for comparisons of the water balance components between these biomes inside the SEALBA region. In addition, local measurements are not suitable for comparisons of water parameters in this region, due to large variations of the environmental conditions making it difficult the implementation of a monitoring system using of long-term series of data (Silva et al., 2023).

To support the rational expansion of crops in areas with agricultural aptitude, as in the case of SEALBA, one can apply methods with the joint use of remote sensing and weather data though algorithms. Because its operationality, the Penman-Monteith (PM) equations has been inserted inside these algorithms for quantification of the water balance components in distinct ecosystems (Cleugh et al., 2007; Nagler et al., 2013; Consoli and Vanella, 2014; Consoli et al., 2016; Olivera-Guerra et al., 2018). When applied together with gridded weather data, the Penman-Monteith equation is suitable for using with low spatial resolution satellite images (Mateos et al., 2013; Vanella et al., 2019). Considering these aspects, the SAFER (Simple Algorithm for Evapotranspiration Retrieving) algorithm was developed for estimations of the water balance components, with simultaneous field and remote sensing measurements in NEB (Teixeira, 2010). The reason for the SAFER's choice in the current research is that besides its applicability, other important advantage, regarding other approaches, is that in its newer version there is no need of the satellite thermal bands, being possible to be used only the visible and the near infrared bands, more easily available than the thermal ones (Consoli and Vanella, 2014). In addition, the thermal bands of the MODIS Terra (EOS AM-1) sensor have a spatial resolution of 1 km, meaning that with their use, the images will cover more pixels with mixed surface types, when comparing with the red and near infrared bands with a 250 m of spatial resolution.

Aiming to implement an operational water balance monitoring system in agricultural growing regions, taking SEALBA as a reference, we tested the last version of the SAFER algorithm with the use of the reflectance MODIS MOD13Q1 product together with long term meteorological data in a period of 15 years (2007–2021). The research, besides contributing by making available water information at the spatial and temporal resolutions of 250 m and 16 days, respectively, will subsidize knowledge of the average water balance conditions and the implementation, refinement and expansion of water resources monitoring systems in the region. The authors believe that the success of these applications in this specific region of NEB will encourage replications of the methods in other environmental conditions of the country and even in other regions of the world, with simple calibrations of the modelling equations.

2. Material and methods

2.1. Study area and meteorological stations

The study area involves the agricultural growing region of the coastal region in NEB, limited by the states Sergipe (SE), Alagoas (AL), and Bahia (BA), called SEALBA, an acronym formed by the initials of these three Brazilian states. Fig. 1 shows the location of SEALBA and its borders, biomes according the Geographic and Statistical Brazilian Institute (IBGE - www.ibge.gov.br), and altitudes,

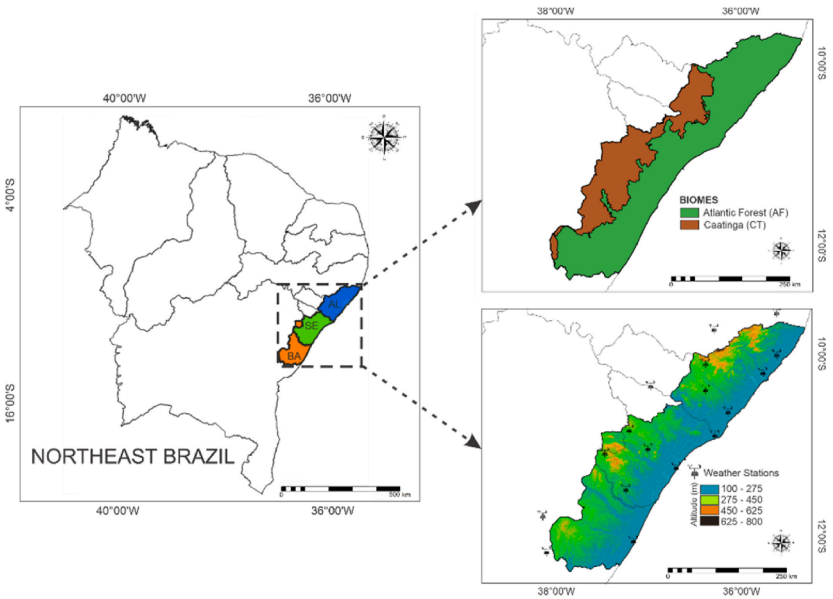

Fig. 1. Location of the SEALBA region in Northeast Brazil (NEB) involving the states of Sergipe (SE), Alagoas (AL), and Sergipe (SE), with details for the biomes, altitudes, and meteorological stations used in the water balance modelling.

together with the 17 meteorological stations used from the National Meteorological Institute (INMET - https://www.gov.br/agricultura/pt-br/assuntos/inmet). The data gaps for some stations in their time series were overcome by covering them with regression equations using the nearest station where data are missed and by geostatistical interpolations applying the moving average method.

Accounting up the MODIS pixels with spatial resolution of 250 m, 33% of SEALBA is in Sergipe – SE (2.0 Mha), 37% is in Alagoas – AL (2.3 Mha), and 30% is in Bahia – BA (1.9 Mha), totalizing 6.2 Mha. The region involves the biomes AF and CT. Most areas in the AF, with 3.9 Mha accounted, mostly below 275 m of altitude, occupies 63% of the SEALBA region, in a portion closer to the coastline. This biome is characterized by forest vegetation, prevailing the rain forest dense and open, the semi-decidual season forest, and ecosystems associated to the coastal lowland. The climate is humid tropical, occasioned by moist air masses coming from the Atlantic Ocean, with high both average air temperature and air humidity and well distributed rainfall along the year (Francisquini et al., 2020). The CT areas, with 2.3 Mha accounted, being the majority above 275 m of altitude, represents 37% of the SEALBA region, presenting species composed by trees and bushes with characteristics that allow climate adaptations. The biome is under high air temperatures but low air humidity with irregular rainfall, associated to long drought periods along the year (Beuchle et al., 2015). Both biomes are suffering by fast replacement of their natural vegetation by crops as fruits, sugar cane, grains, forestry, and pasture (Beuchle et al., 2015; Procopio et al., 2019).

The input meteorological data for the large-scale water balance modelling were incident global solar radiation (R_G); air temperature (T_a), air relative humidity (RH), and wind speed (u); for the calculation of reference (ET_0) and actual (ET) evapotranspiration. To account the water balance, precipitation (P) data were also used together with the modeled ET (Teixeira et al., 2020; 2021). With a geographic information system (GIS) these data were layered with the remote sensing parameters by using the geostatistical interpolation method of "moving average", contributing to a better spatial characterization of the water balance components.

2.2. Characteristics of the MODIS images

For large-scale modelling the water balance components in the SEALBA region, it was used the bands 1 and 2 from the MODIS sensor (MOD13Q1 reflectance product) downloaded from the site of EARTHDATA Aρρ EEARS (https://lpdaacsvc.cr.usgs.gov/appeears/), together with the meteorological stations from INMET. Table 1 presents the characteristics of the MODIS bands 1 (B1) and 2 (B2) from the MOD13Q1 reflectance product with the respective spectral ranges, sweep length, and spatial/temporal resolutions.

MODIS is a sensor onboard Terra and Aqua platforms, having 36 spectral bands between 0.405 and 14,385 μm, which collects data at three spatial resolutions (250, 500 and 1000 m). The MODIS MOD13Q1 reflectance product, has spatial and temporal resolu-

Table 1
Characteristics of the bands 1 and 2 from the MODIS MOD13Q1 reflectance product used for modelling the water balance components in the SEALBA region, Northeast Brazil.

Sensor	MODIS product	Bands	Spectral range (μm)	Sweep length (km)	Spatial resolution (m)	Temporal resolution (day)
MODIS	MOD13Q1	B1	0.62–0.67	2330	250	16
		B2	0.84–0.87			

tions of 250 m and 16 days, respectively, giving 23 free-cloud images of along a year, which together with meteorological data, allowed to model the dynamics of water balance components with the newest version of the SAFER algorithm, without thermal bands. In the current paper, the 16-day reflectance values from the MODIS Terra (EOS AM-1) sensor were grouped and coupled with time up scaled gridded weather data for quarter and annual water balance analyses in the AF and CT biomes inside the SEALBA region.

2.3. Water balance modelling

Fig. 2 shows a schematic view of the SAFER algorithm, applied with the MODIS MOD13Q1 reflectance product and meteorological data, to estimate the water balance components in the SEALBA region ran from 2007 to 2021.

All the regression coefficients of the equations for the parameters decribed in Fig. 2 were determined by simultaneous satellite and field measurents in the NEB involving natural vegetation and irrigated crops under strongly contrasting thermohydrological conditions (Teixeira, 2010; Teixeira et al., 2008; 2013). After elaboration, the SAFER algorithm has been validated in several Brazilian agroecosystems of the NEB (Araujo et al., 2019; Leivas et al., 2017; Silva et al., 2019; Teixeira et al., 2020; 2021). Besides these validations, the main equation for evaporative fraction (ET_f) values were satisfactorily checked with literature. Thus, one can expect enough accuracy for our objective of testing an operational monitoring system, with comparisons among the AF and CT biomes being replaced by crops, giving a first insight of the spatial and temporal dynamics for the water balance components, being not strictly necessary new expensive simultaneous field and satellite measurements in the SEALBA region.

Following Fig. 2, the surface albedo (α_0) pixel values were calculated as:

$$\alpha_0 = a + b\rho_1 + c\rho_2 \quad (1)$$

where ρ_1 e ρ_2 are respectively the MODIS reflectance from bands 1 (red) and 2 (near infra-red); a, b, and c are regression coefficients. In NEB, the coefficients a, b, and c were 0.08, 0.41, and 0.14, involving irrigated crops and natural vegetation under contrasting hydrological conditions, which can be calibrated for specific environments if more accuracy for α_0 is desirable (Teixeira et al., 2008; 2013).

The Normalized Difference Vegetation Index (NDVI) is used as a surface cover and root-zone moisture conditions remote-sensing parameter:

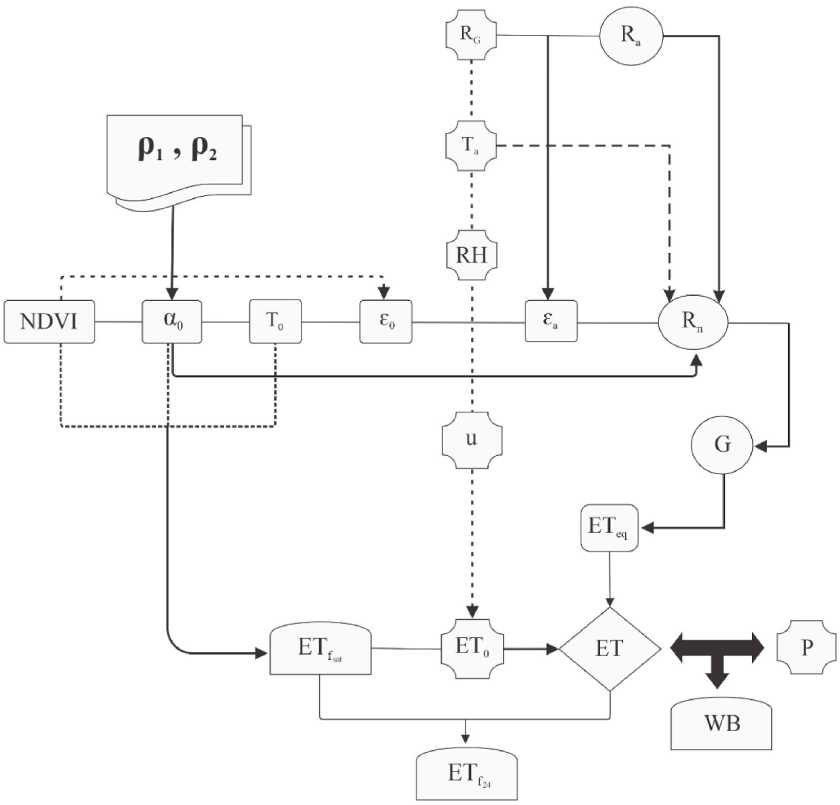

Fig. 2. Flowchart for application of the SAFER algorithm with the MODIS MOD13Q1 reflectance product and meteorological data, to assess the water balance components in the SEALBA region, ran from 2007 to 2021.

$$NDVI = \frac{\rho_2 - \rho_1}{\rho_2 + \rho_1} \quad (2)$$

Net radiation (R_n) was estimated through the Slob equation (de Bruin 1987):

$$R_n = (1 - \alpha_0) R_G - a_L \tau_{sw} \quad (3)$$

where τ_{sw} is the short-wave atmospheric transmissivity and a_L is a regression coefficient up scaled throughout the mean air temperature (T_a) pixel values.

$$a_L = a_T T_a + b_T \quad (4)$$

and the regression coefficients a_T and b_T for NEB were found to be 6.8 and −40, respectively, but they can be adjusted for specific environmental conditions with field radiation balance measurements (Teixeira et al., 2008; Teixeira, 2010).

The atmospheric emissivity (ϵ_A) was calculated according to Teixeira et al. (2020, 2021):

$$\varepsilon_A = a_A (\ln \tau_{sw})^{b_A} \quad (5)$$

where a_A and b_A are regression coefficients, which are reported as 0.94 and 0.11, respectively, for NEB, but they can be calibrated with field radiation balance measurements for specific environmental conditions (Teixeira et al., 2008, 2013).

The surface emissivity (ϵ_0) was estimated according to Rampazo et al. (2020) and Silva et al. (2019):

$$\varepsilon_0 = a_0 \ln NDVI + b_0 \quad (6)$$

where a_0 and b_0 are regression coefficients, which were reported as 0.06 and 1.00 for NEB, but they can be acquired for specific environmental conditions by simultaneous field radiation balance and NDVI remote sensing measurements (Teixeira et al., 2008; Teixeira, 2010).

By the residual method, following the physical principle of the Stefan-Boltzmann' low, T_0 was estimated as:

$$T_0 = \frac{\sqrt[4]{R_G (1 - \alpha_0) + \sigma \varepsilon_a T_a^4 - R_n}}{\sigma \varepsilon_0} \quad (7)$$

where $\sigma = 5.67\ 10^{-8}$ W m^{-2} K^{-4} is the Stefan-Boltzmann constant.

To estimate the actual evapotranspiration (ET), its ratio to the reference evapotranspiration (ET_0), i.e., the evapotranspiration fraction at the satellite overpass time ($ET_{f_{sat}}$), was modeled:

$$ET_{f_{sat}} = \exp\left[a_{sf} + b_{sf}\left(\frac{T_0}{\alpha_0 NDVI}\right)\right] \quad (8)$$

where the regression coefficients a_{sf} and b_{sf} found for NEB were 1.90 and −0.008 (Teixeira et al., 2008; Teixeira, 2010), being possible to be calibrated through field measurements of ET and ET_0 and the remote sensing parameters α_0, NDVI e T_0 in contrasting hydrological surfaces (Safre et al., 2022; Venâncio et al., 2021).

Eq. (8) does not work for water bodies or mixture of land and water (NDVI < 0), thus, the concept of equilibrium evapotranspiration - ET_{eq} (Raupasch, 2001) is used in the SAFER algorithm under these circumstances:

$$ET_{eq} = 0.035\left(\frac{\Delta (R_n - G)}{\Delta + \gamma}\right) \quad (9)$$

where Δ is the inclination of the curve relating the saturation vapor pressure (e_s) and T_a, γ is the psychrometric constant, and G is the ground heat fluxes estimated according:

$$\frac{G}{R_n} = a_G \exp(b_G \alpha_0) \quad (10)$$

being a_G and b_G regression coefficients, found to be 3.98 and −25.47, respectively, for the NEB, but can be calibrated with simultaneous field energy balance measurements for other environmental conditions (Teixeira et al., 2008, 2013).

Considering that the satellite overpass values of the evapotranspiration fraction does not differ so much from the daily ones (Allen et al., 2007), throughout conditional functions applied to the NDVI values, the daily ET pixel values were estimated as:

$$ET = ET_{f_{sat}} ET_0 \text{ou} ET_{eq} \quad (11)$$

being ET_0 calculated by using the gridded daily weather data on incident global solar radiation (R_G), mean air temperature (T_a), relative humidity (RH), and wind speed (u) (Allen et al., 1998).

After retrieving ET on large scale, including water bodies, the daily values of $ET_{f_{24}}$ was acquired:

$$ET_{f_{24}} = \frac{ET}{ET_0} \tag{12}$$

Similarly, to what was done in Australia (Cleugh et al., 2007) and in Southeast Brazil (Teixeira et al., 2017), the water balance (WB) was computed as:

$$WB = P - ET \tag{13}$$

where P is the gridded precipitation values from the net of weather stations.

To relate the water parameters, precipitation (P), actual evapotranspiration (ET), water balance (WB), and evaporative fraction (ET_f) in the Atlantic Forest (AF) and Caatinga (CT), the Pearson correlation coefficient (r) was used.

3. Results and discussion

3.1. Spatial and temporal dynamics of precipitation

Fig. 3 presents the spatial distributions of the mean total values of P for some of the MODIS 16-day periods along the year, together with the average pixel values and standard deviations (SD) regarding the biomes AF and CT, inside the SEALBA region from 2007 to 2021, in terms of Day of the Year (DOY).

In general, for both biomes, AF and CT, inside the SEALBA region, the rainfall distributions along the year are spatially and temporally irregular, however lower P values are for CT when compared with those for AF, mainly from April to July (DOY 097–192), when the 16-day average difference between these biomes was above 12 mm. During this period occur the P maximums, with 16-day average total above 60 mm in AF and higher than 50 mm in CT. The lowest P values, with 16-day average total bellow 15 mm in both biomes, are in December (DOY 321–336). Regarding the annual scale, the mean total in CT, with 772 mm yr^{-1}, is 83% of that for AF (927 mm yr^{-1}). According to the standard deviations (SD) along the year, it is noticed higher spatial variations for AF than for CT,

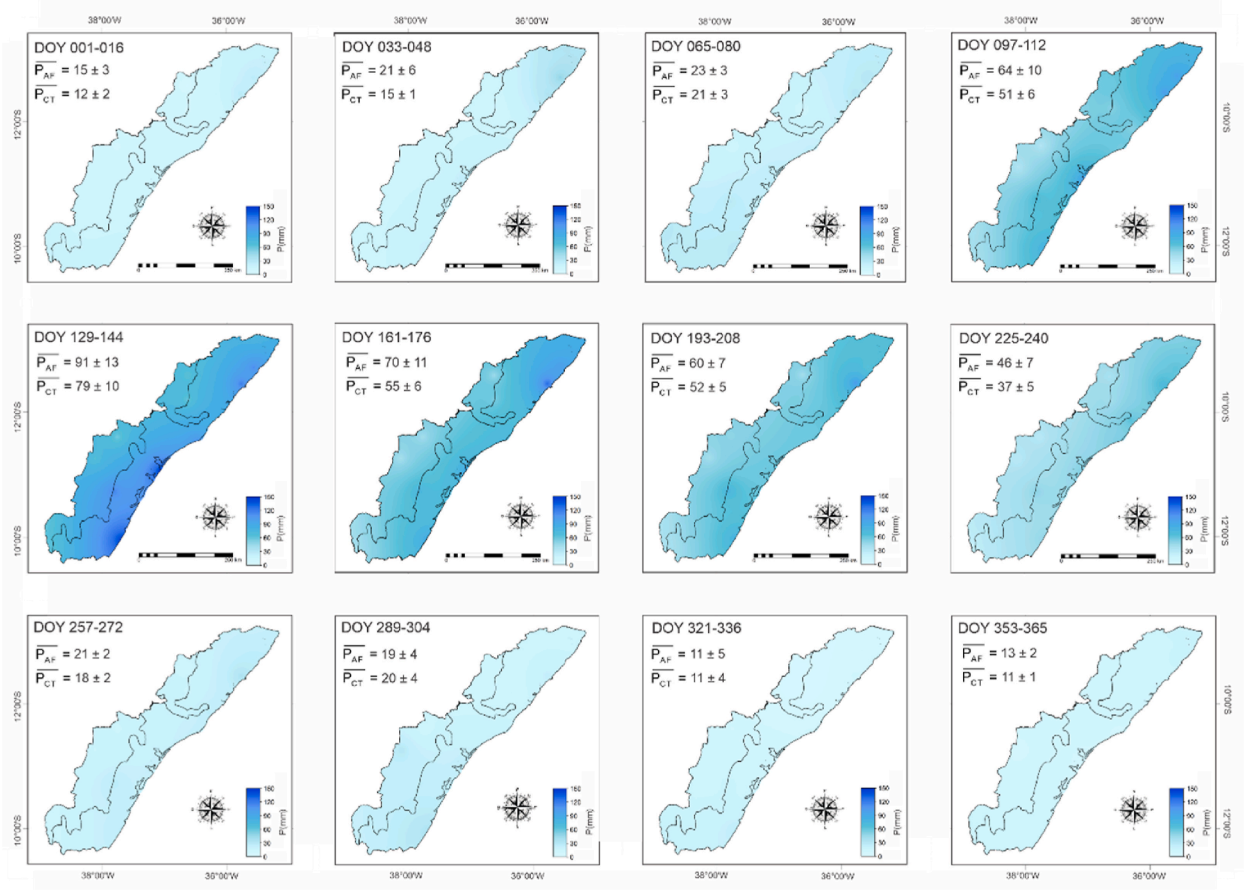

Fig. 3. Spatial distributions of the mean totals for precipitation (P), at some MODIS 16-day intervals along the year in the SEALBA region, together with the average pixel values and standard deviations (SD), from 2007 to 2021 for the biomes Atlantic Forest (AF) and Caatinga (CT), in terms of Day of the Year (DOY).

with SD representing 17 and 14% of the average pixel values, respectively. According to Filho et al. (2019) anthropogenic processes and natural variability interfere with the forms of rain interception in these biomes inside NEB and hence in their rainfall patterns.

Accounting the MODIS pixels of 250 × 250 m in the AF and CT biomes inside the states of Sergipe (SE), Alagoas (AL) and Bahia (BA) limited by the SEALBA region (see Fig. 1), the areas with AF account for 62, 78, and 46% of these states, respectively. Regarding the CT biome, the corresponding percentages are 38, 22, 54%. Larger areas with AF biome than for the CT one inside the SEALBA region promote higher P rates in the Alagoas, followed by Sergipe and Bahia.

From water balance measurements in the AF biome during 2008, Pereira et al. (2010), reported an annual P value of 1313 mm yr^{-1}. According to Silva et al. (2023) AF in the coastal zone of NEB, with the availability of moisture from the Atlantic, presents a total annual rainfall ranging from 1000 to 2400 mm yr^{-1}. These values are a little higher than our annual average total of 997 mm yr^{-1}. Silva et al. (2017) found a P annual value in the CT biome of 430 mm yr^{-1} from 2014 to 2015, lower than our long-term value of 772 mm yr^{-1}. However, also in the CT biome, Oliveira et al. (2022) reported an average annual P value of 783 mm yr^{-1}, very close to our annual value for this biome. As P values of the current study for AF and CT biomes are averages over 15 years, it is observed that the rainfall amounts for specific years should vary to above or below regarding their long-term values. Analyzing the dynamics of rainfall at 16-day periods along the year, both the AF and CT biomes inside the SEALBA region present two defined seasons, one drier and the other rainier, with the highest amounts concentrated in the middle of the year.

3.2. Spatial and temporal dynamics of actual evapotranspiration

Fig. 4 shows the spatial distributions of the mean daily rates of actual evapotranspiration (ET) for some of the MODIS 16-day periods along the year in the SEALBA region, together with the average pixel values and standard deviations (SD) regarding the biomes AF and CT from 2007 to 2021, in terms of day of the year (DOY).

As for P, large spatial and temporal variations on ET values are observed along the year inside the SEALBA region. The highest values happen between July and September (DOY 193–256), when the 16-day average surpass 2.70 mm d^{-1} for the AF biome and 2.90 mm d^{-1} in the CT biome. The lowest ET rates occur from January to February, when the 16-day averages in AF are lower than 1.50 mm d^{-1} and bellow 1.00 mm d^{-1} in CT. At the annual scale the mean totals are 760 and 601 mm yr^{-1} for respectively AF and CT, with the rates in CT being 79% of those for AF.

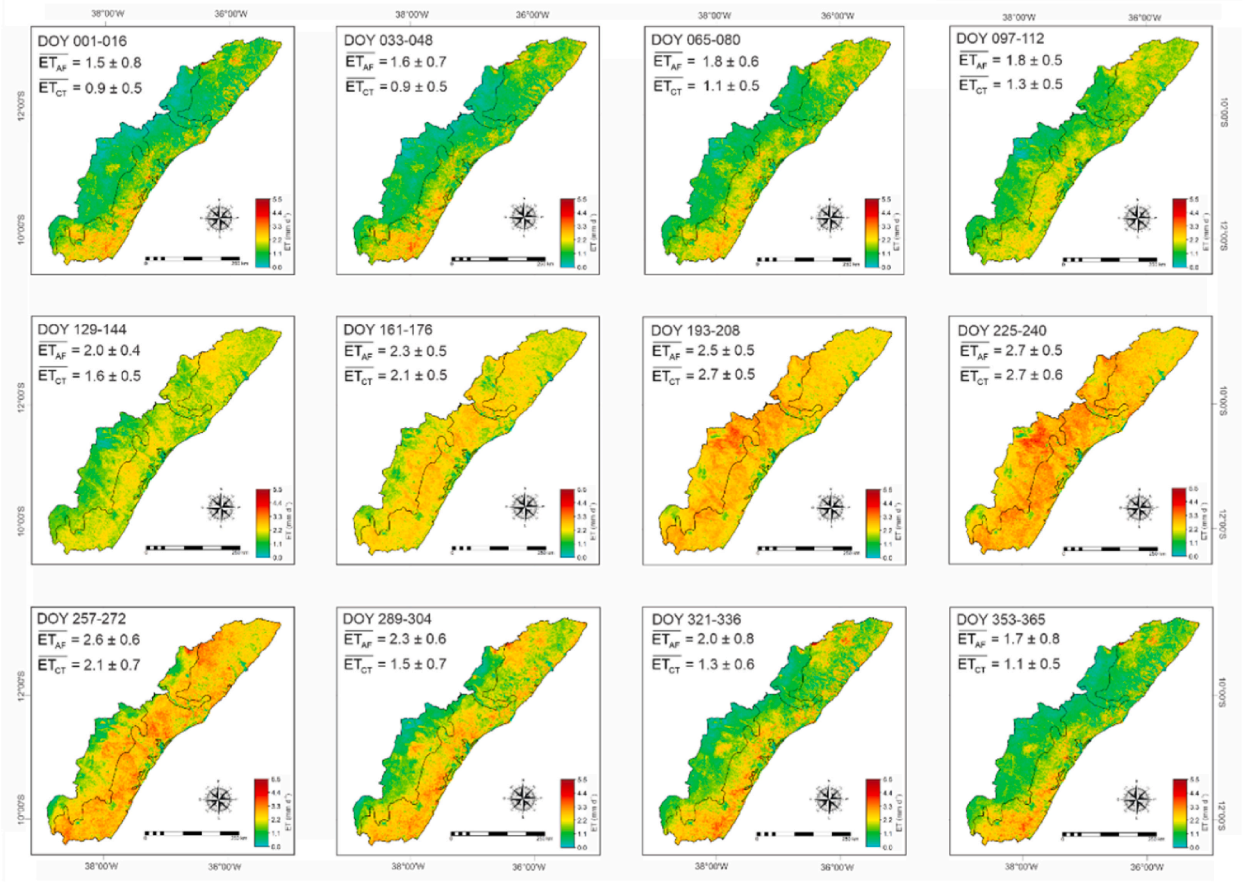

Fig. 4. Spatial distributions of the mean daily rates of actual evapotranspiration (ET), at some MODIS 16-day intervals in the SEALBA region, together with the average pixel values and standard deviations (SD) from 2007 to 2021 for the biomes Atlantic Forest (AF) and Caatinga (CT), in terms of day of the year (DOY).

Trough the soil water balance method in the AF biome, at the annual scale, Pereira et al. (2010) reported a daily average ET of 3.20 mm d^{-1}, a little higher than our one of 2.08 ± 0.59 mm d^{-1} for this biome. However, with the same water balance techniques between 2013 and 2018 in AF, Rodrigues et al. (2021) found ET average values ranging from 1.40 a 1.80 mm d^{-1} under drought conditions, like our values under the driest periods at the beginning and at the end of the year. From energy balance measurements from 2014 to 2015, using the eddy covariance method in the CT biome, Silva et al. (2017) found daily ET average values ranging from 0.98 mm d^{-1} during the dry season to 1.96 mm d^{-1} in the rainy season. Also, with eddy covariance measurements in CT from 2014 to 2015, Marques et al. (2020) reported daily average ET rates from 0.20 to 0.30 mm d^{-1}, during the dry season till the range from 1.70 to 2.60 mm d^{-1} in the rainy season. These rates involve our ones considering the average pixel values and standard deviations, with an annual average value of 1.65 ± 0.54 mm d^{-1}.

The rainfall amounts are the main evapotranspiration driving forcing in both biomes inside the SEALBA region, explaining the different ET rates between the AF and CT biomes. However, one must consider that other important reason for these differences can be related to differences on the soil cover by vegetation, affecting the absorbed solar radiation and the ET partition into transpiration and soil evaporation (Villalobos et al., 2013). On the other hand, Filho et al. (2021), pointed out that air temperature, air humidity, wind speed, and solar radiation influence the ET rates in NEB. In general, the ET ranges for the AF and CT biomes inside the SEALBA region found in the current study, are reasonably comparable to those from literature, even under different rainfall conditions for specific periods.

3.3. Large-scale water balance

For the water balance – WB (Eq. (13)), the daily average ET values were up scaled to 16-day average totals. Fig. 5 presents the average WB pixel values together with the standard deviations (SD) at this temporal scale along the year, for the AF and CT biomes, inside the SEABA region, from 2007 to 2021, in terms of day of the year (DOY).

For the AF biome, the highest 16-day positive WB of 61 mm, occur under the largest P of 92 mm at a corresponding ET of 31 mm in May (DOY 129–144). The most negative WB, with a 16-day value of −21 mm happen in September (DOY 257–272), with P of 21 mm under a high ET of 42 mm. At the annual scale, in the AF biome WB was 164 mm. The periods with maximum and minimum WB for CT are also respectively in May (DOY 129–144), with WB of 55 mm at P of 80 mm and ET of 25 mm, and September (DOY 257–272), when WB is −16 mm at P of 18 mm and ET of 34 mm. The largest positive16-day value in CT was 55 mm, under conditions of high P of 80 mm and low ET of 25 mm, while the most negative one was −16 mm under P of 18 mm at a high ET of 34 mm. At the annual scale, CT with WB of 168 mm, has a slightly higher rainfall water availability than that for AF, with a difference of 2%, because even the AF having higher rainfall amounts, its higher water fluxes reduce WB when comparing with the CT biome. One must also to consider that the CT covering more dry conditions is much larger than the areas inside the SEALBA region which involve transitions between this biome and AF.

High rainfall amounts together with low water vapor transfer concentrates the positive WB from March to August (DOY 081–224) for both biomes, AF and CT, inside the SEALBA region, what is favorable for the rainfed agriculture. However, from the end of July to the second half of December (DOY 209–265) occur the negative WB values, indicating the need of irrigation for critical crop stages. The respective lowest and highest ET rates, are explained by the lowest and highest rainfall amounts, respectively, but when the root-zone moisture is not a limiting factor, as in the middle of the year, when there is high rainfall water availability, the largest ET rates for CT in some occasions can be due to higher available energy when comparing with AF (Seneviratne et al., 2010), since none of these biomes are under rainfall water scarcity during this period inside the SEALBA region.

To infer the root-zone moisture conditions in the water balance along the year, Fig. 6 shows the daily average values of the evaporative fraction ($\mathbf{ET}_{f_{24}}$) at the MODIS 16-day interval along the year, together with the standard deviations (SD) for the biomes AF and CT, inside the SEALBA region, from 2007 to 2021, in terms of day of the year (DOY).

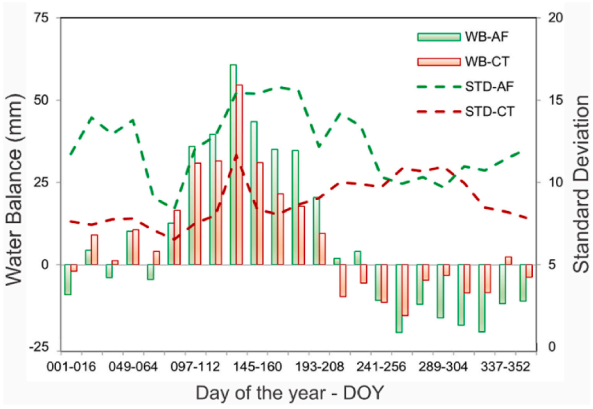

Fig. 5. Average MODIS 16-day values and standard deviations (SD) of the water balance (WB) along the year, for the biomes Atlantic Forest (AF) and Caatinga (CT) inside the SEALBA region, from 2007 to 2021, in terms of day of the year (DOY).

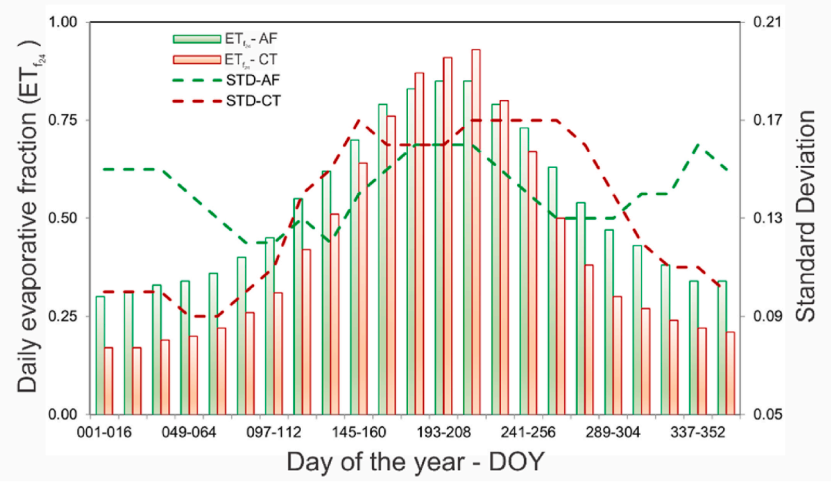

Fig. 6. Average daily values for the evaporative fraction ($ET_{f_{24}}$) at the MODIS 16-day intervals along the year, for the biomes Atlantic Forest (AF) and Caatinga (CT) inside the SEALBA region, from 2007 to 2021, in terms of day of the year (DOY).

The highest $\mathbf{ET}_{f_{24}}$ values for the AF biome, above 0.50. Happen from the April to October (DOY 113–288), while for the CT these high values occur from May to September (DOY 129–272). Although at the annual scale the $\mathbf{ET}_{f_{24}}$ average value for AF is 21% larger than that for CT ($\mathbf{ET}_{f_{24}} = 0.44$), comparing the maximums between these biomes during the rainy season from July to August (DOY 209–224), it is observed an $\mathbf{ET}_{f_{24}}$ value of 0.93 for CT while in the AF biome it is 0.85, a difference of 9%. The lowest $\mathbf{ET}_{f_{24}}$ values for AF, bellow 0.40, are from November to March (DOY 001–080 and DOY 321–365), while for CT the minimums ones, lower than 0.30, are from October to April (DOY 001–096 and DOY 321–365). The lowest values happen are in the beginning of the year, in January (DOY 001–016), for both biomes, however the average for AF of 0.30 is 76% higher than those for CT, which presents a mean value of 0.17 during this period.

In well-irrigated crops, the $\mathbf{ET}_{f_{24}}$ values are called crop coefficients (K_c) and can be used for crop water requirements estimations (Teixeira et al., 2018). On the other hand, under condition of non-optimum root-zone moisture, it can characterize the degree of water stress (Lu et al., 2011). According to Mateos et al. (2013), the $\mathbf{ET}_{f_{24}}$ values in plants under water scarcity conditions are most influenced by the stomata aperture, what is the case of the CT species under the driest conditions. Thus, considering agricultural growing areas in the SEALBA region, the $\mathbf{ET}_{f_{24}}$ values found in the current study from April to September, indicate this period as the most favorable for rainfed crops, and in some cases, with better conditions for CT when compared to the AF biome. However, from October to April, the lower $\mathbf{ET}_{f_{24}}$ values in CT are directly related to drops on the root-zone water availability for plants, because of lower rainfall amounts associated to high atmosphere demand.

In pastures from Florida (USA), Sumner and Jacobs (2005) reported $ET_{f_{24}}$ values ranging from 0.47 to 0.92 under irrigation conditions, while in steppes under desertic conditions of Mongolia, China, Zhang et al. (2012) found a $ET_{f_{24}}$ range from 0.16 to 0.75. These values are similar in several situations depicted in Fig. 6, for both AF and CT biomes. According to Zhou and Zhou (2009), the climate variables which most affect $ET_{f_{24}}$ are air temperature, air humidity, and the available energy, as they affect both ET and ET_0 (Filho et al., 2021). However, the values of this root-zone moisture indicator will also depend on the stomata aperture and adaptation of species to water scarcity (Mata-González et al., 2005), what is much visible for the CT than for AF biome inside the SEALBA region.

Comparing the WB values (Fig. 5) with those for $ET_{f_{24}}$ (Fig. 6), and considering both biomes, AF and CT, inside the SEALBA region, it is noticed that while the highest root-zone moisture conditions, with $ET_{f_{24}}$ values (above 0.50) occur from the end of April to October (DOY 113–288). Regarding the water balance, the highest WB values (above 14 mm) are from March to August (DOY 081–240). Therefore, there is a delay till two months between the moment in which rainfall attend evapotranspiration with that in which the root-zone moisture recovers its optimum level after a dry period.

3.4. Statistical analyses

Table 2 shows the results for the Pearson correlation coefficients, relating the values for precipitation (P), evapotranspiration (ET), water balance (WB), and evaporative fraction (ET_f) values in Atlantic Forest versus those for Caatinga. Also, it presents the correlation between P and ET, and BH and ET_f for each biome.

According to Table 2, all water parameters in Atlantic Forest (AF) had strong positive correlations with those in Caatinga (CT). However, when relating P with ET in both biomes with the correlations weak in AF and moderate in CT. The same behavior was for WB and ET_f between biomes, being the correlations moderate when relating WB with ET_f in AF and weak comparing these water parameters in CT. However, the relationships P with ET and WB with ET_f n AF, and WB with ET_f in CT were not statistically significant at $p > 0.05$. The reasons for the low correlations in Table 2 may be explained by a gap between P and ET values along the year, which could be related to the time needed for recovering good soil moisture after rainfalls, but also because of some rainfall water is lost by runoff and percolation.

Table 2
Pearson correlation coefficients between precipitation (P), actual evapotranspiration (ET), water balance (WB), and evaporative fraction (ETf) in the Atlantic Forest (AF) and Caatinga (CT) biomes.

Variables/Coefficient	$\mathbf{P_{AF}}$*$\mathbf{P_{CT}}$	$\mathbf{ET_{AF}}$*$\mathbf{ET_{CT}}$	$\mathbf{P_{AF}}$*$\mathbf{ET_{AF}}$	$\mathbf{P_{CT}}$*$\mathbf{ET_{CT}}$
r	0.99	0.93	0.22	0.43
Variables/Coefficient	WB_{AF}*WB_{CT}	$ET_{f_{AF}}$*$ET_{f_{CT}}$	WB_{AF}*$ET_{f_{AF}}$	WB_{CT}*$ET_{f_{CT}}$
r	0.94	0.99	0.41	0.09

Water variables: Precipitation (P), Actual Evapotranspiration (ET), Water Balance (WB), and Evaporative Fraction.
Biomes: Atlantic Forest (AF) and Caatinga (CT).

4. Conclusions

It was demonstrated that the SAFER algorithm is feasible to be applied with the MODIS MOD13Q1 reflectance product and gridded meteorological data to monitor water balance components in agricultural growing regions with different biomes and agricultural consortium, as in the case of SEALBA. Inferring the root-zone moisture conditions through the evaporative fraction, it noticed by its highest values, that the best moisture levels for plants are from April to September, being this period suitable for rainfed agriculture, with some cases happening better conditions in the driest Caatinga biome than those for the wettest Atlantic Forest biome. The lowest values of the evaporative fraction in the biome Caatinga, from October to April, are directly related to less availability of root-zone moisture when comparing with Atlantic Forest.

According to Pearson correlation coefficient, all analyzed water parameters in Atlantic Forest (AF) had strong positive correlations with those in Caatinga (CT). However, when relating precipitation (P) with actual evapotranspiration in both biomes the correlations were weak in AF and moderate in CT. The same behavior was for water balance (WB) and evaporative fraction (ET_f) between biomes, being the correlations moderate when relating their relation in AF and weak in CT. However, the relationships P with ET and WB with ET_f n AF**,** and also WB with ET_f in CT were not statistically significant at $p > 0.05$. The reasons for the low correlations in Table 2 may be explained by a gap between P and ET values along the year, which could be related to the time needed for recovering good soil moisture after rainfalls, but also because of some rainfall water is lost by runoff and percolation.

Although we tested the models for a specific region in the coast of Northeast Brazil, the applicability of the joint use of the MODIS MOD13Q1 reflectance product with gridded weather data presents strong potential for implementation of an operational system to monitor the water balance components in any environmental conditions. Future research can focus on detecting of water balance anomalies for specific years comparing with long-term conditions, subsidizing public policies regarding the management and conservation of water resources, mainly under the actual scenarios of climate and land use changes. Limitations for applications of the methods in other environments could be lack of meteorological data on large-scales and the possible need of calibration of the equations which demand simultaneous field and satellite measurements.

Funding

This research did not receive any specific grant from funding agencies in the public, commercial, or not-for-profit sectors.

Author contributions

Franzone Farias – Was responsible for running the models, conceptualizations, water balance assessments, writing the manuscript, designing of figures, result analyses, software resources. Antônio Teixeira – Oversaw running of scripts, download and processing MODIS images MODIS images, formatting of the weather data, methodology, data curation, editing of the manuscript and supervision. Inajá Sousa – Helped on downloading and processing MODIS images, weather data processing, and result analyses. Janice Leivas – Helped on downloading and processing MODIS images, weather data processing, and result analyses. Edlene Garçon – Acted on downloading/processing MODIS images and weather data.

Declaration of competing interest

The authors declare that they have no known competing financial interests or personal relationships that could have appeared to influence the work reported in this paper.

Data availability

Data will be made available on request.

Acknowledgements

To National Meteorological Institute (INMET) for meteorological data availability.

References

Akhtar, N., Syakir Ishak, M.I., Bhawani, S.A., Umar, K., 2021. Various natural and anthropogenic factors responsible for water quality degradation: a review. Water 13, 2660.

Allen, R.G., Pereira, L.S., Raes, D., Smith, M., 1998. Crop evapotranspiration, Guidelines for computing crop water requirements. In: FAO Irrigation and Drainage Paper 56. Rome, Italy.

Allen, R.G., Tasumi, M., Morse, A., Trezza, R., Wright, J.L., Bastiaanssen, W.G.M., Kramber, W., Lorite, I., Robison, C.W., 2007. Satellite-based energy balance for mapping evapotranspiration with internalized calibration (METRIC) - applications. J. Irrigat. Drain. Eng. 133, 395–406.

Araujo, L.M., Teixeira, A.H. de C., Bassoi, L.H., 2019. Evapotranspiration and biomass modelling in the pontal sul irrigation scheme. Int. J. Rem. Sens. 1, 1–13.

Asokan, A., Anitha, J., Ciobanu, M., Gabor, A., Naaji, A., Hemanth, D.J., 2020. Image processing techniques for analysis of satellite images for historical maps classification-an overview. Appl. Sci. 10, 4207.

Beuchle, R., Grecchi, R.C., Shimabukuro, Y.E., Seliger, R., Eva, H.D., Sano, E., Achard, F., 2015. Land cover changes in the Brazilian Cerrado and Caatinga biomes from 1990 to 2010 based on a systematic remote sensing sampling approach. Appl. Geogr. 58, 116–127.

Cleugh, H.A., Leuning, R., Mu, Q., Running, S.W., 2007. Regional evaporation estimates from flux tower and MODIS satellite data. Remote Sens. Environ. 106, 285–304.

Consoli, S., Vanella, D., 2014. Comparisons of satellite-based models for estimating evapotranspiration fluxes. J. Hydrol. 513, 475–489.

Consoli, S., Licciardello, F., Vanella, D., Pasotti, L., Villani, G., Tomei, F., 2016. Testing the water balance model CRITERIA using TDR measurements, micrometeorological data, and satellite-based information. Agric. Water Manag. 170, 68–80.

de Bruin, H.A.R., 1987. From penman to makkink. In: Hooghart, J.C. (Ed.), Proceedings and Information: TNO Committee on Hydrological Sciences, vol. 39. Gravenhage, The Netherlands, pp. 5–31.

Filho, W.L.F.C., Oliveira-Júnior, J.F. de, Santiago, D. de B., Terassi, P.M. de B., Teodoro, P.E., De Gois, G., Blanco, C.J.C., Souza, P.H. de A., Costa, M. da S., Gomes, H.B., Dos Santos, P.J., 2019. Rainfall variability in the Brazilian northeast biomes and their interactions with meteorological systems and ENSO via CHELSA product. Big Earth Data 3/4, 315–337.

Filho, W.L.F.C., Santos, T.V., dos Santiago, D.B., Oliveira-Junior, J.F. de, Amorim, R.F.C., 2021. Influence of meteorological variables on reference evapotranspiration in the State of Alagoas, Brazil, based on multivariate analysis. Model. Earth Syst. Environ. 7, 2215–2224.

Francisquini, M.I., Lorente, F.L., Pessenda, L.C.R., Junior, A.A.B., Mayle, F.E., Cohen, M.C.L., França, M.C., Bendassolli, J.A., Giannini, P.C.F., Schiavo, J.A., Macario, K., 2020. Cold and humid Atlantic Rainforest during the last glacial maximum, northern Espírito Santo state, southeastern Brazil. Quat. Sci. Rev. 244, 106489.

IPCC, 2023. Climate change 2023: synthesis report. In: Lee, H., Romero, J. (Eds.), A Report of the Intergovernmental Panel on Climate Change. Contribution of Working Groups I, II and III to the Sixth Assessment Report of the Intergovernmental Panel on Climate Change. IPCC, Geneva, Switzerland. (in press).

Jardim, A.M.R.F., Júnior, G.N.A., da Silva, M.V., dos Santos, A., da Silva, J.L.B., Pandorfi, H., Oliveira-Júnior, J.F. de, Teixeira, A.H. de C., Teodoro, P.E., de Lima, J.L.P.M., Junior, C.A.S., Souza, L.S.B., Silva, E.A., Silva, T.G.F.S., 2022. Using remote sensing to quantify the joint effects of climate and land use/land cover changes on the Caatinga biome of Northeast Brazilian. Rem. Sens. 14, 1911.

Kamble, B., Kilic, A., Hubard, K., 2013. Estimating crop coefficients using remote sensing-based vegetation index. Rem. Sens. 5, 1588–1602.

Leivas, J.F., Teixeira, A.H. de C., Silva, G.B., Garçon, E.A.M., Ronquim, C.C., 2017. Water indicators based on SPOT 6 satellite images in irrigated area at the Paracatu River Basin, Brazil. Proc. SPIE 1042, 104211I. . 1 - 104211I-7.

Lu, N., Chen, S., Wilske, B., Sun, G., Chen, J., 2011. Evapotranspiration and soil water relationships in a range of disturbed and undisturbed ecosystems in the semi-arid Inner Mongolia, China. J. Plant Ecol. 4, 49–60.

Marques, T.V., Mendes, K., Mutti, P., Medeiros, S., Silva, L., Perez-Marin, A.M., Campos, S., Lúcio, P.S., Lima, K., Reis, J., dos Ramos, T.M., Silva, D.F. da, Oliveira, C.P., Costa, G.B., Antonino, A.C.D., Menezes, R.S.C., Santos e Silva, C.M., Bergson Bezerra, B., 2020. Environmental and biophysical controls of evapotranspiration from seasonally dry tropical forests (Caatinga) in the Brazilian Semiarid. Agric. For. Meteorol. 287, 107957.

Mata-González, R., McLendon, T., Martin, D.W., 2005. The inappropriate use of crop transpiration coefficients (K_c) to estimate evapotranspiration in arid ecosystems: a review. Arid Land Res. Manag. 19, 285–295.

Mateos, L., González-Dugo, M.P., Testi, L., Villalobos, F.J., 2013. Monitoring evapotranspiration of irrigated crops using crop coefficients derived from time series of satellite images. I. Method validation. Agric. Water Manag. 125, 81–91.

Nagler, P.L., Glenn, E.P., Nguyen, U., Scott, R.L., Doody, T., 2013. Estimating riparian and agricultural actual evapotranspiration by reference evapotranspiration and MODIS enhanced vegetation index. Rem. Sens. 5, 3849–3871.

Nyolei, D., Nsaali, M., Minaya, V., van Griensven, A., Mbilinyi, B., Diels, J.H., Kahimba, F., 2019. High resolution mapping of agricultural water productivity using SEBAL in a cultivated African catchment, Tanzania. Phys. Chem. Earth 112, 36–39.

Olivera-Guerra, L., Merlin, O., Er-Raki, S., Khabba, S., Escorihuela, M.J., 2018. Estimating the water budget components of irrigated crops: combining the FAO-56 dual crop coefficient with surface temperature and vegetation index data. Agric. Water Manag. 208, 120–131.

Oliveira, M.L., Santos, C.A.C. dos, Oliveira, G., de Silva, M.T., Silva, B.B. da, Cunha, J.E.B.L., Ruhoff, A., Santos, C.A.G., 2022. Remote sensing-based assessment of land degradation and drought impacts over terrestrial ecosystems in Northeastern Brazil. Sci. Total Environ. 835, 155490. 2022.

Oliveira-Júnior, J.F. de, Shah, M., Abbas, A., Filho, W.L.F.C.F., Junior, C.A.S., Santiago, D.B., Teodoro, P.E., Mendes, D., Souza, A., de Aviv-Sharon, E., Silveira, V.R., Pimentel, L.C.G., Silva, E.B. da, Mohd, A.H., Khan, I., Abdullah, M.A., Attia, E.-A., 2022. Spatiotemporal analysis of fire foci and environmental degradation in the biomes of northeastern Brazil. Sustainability 14, 6935.

Pereira, D.R., Mello, C.R., de Silva, A.M. da, Yanagi, S.N.M., 2010. Evapotranspiration and estimation of aerodynamic and stomatal conductance in a fragment of Atlantic Forest in Mantiqueira range region, MG. Cerne 16, 32–40.

Procopio, S. de O., Cruz, M.A.S., Almeida, M.R.M. de, Junior, Jesus, de, L.A., Junior, Nogueira, L, R., Carvalho, H.W.L. de, 2019. Sealba: região de alto potential agrícola no Nordeste brasileiro. Aracaju: embrapa Tabuleiros Costeiros. 2019. In: Embrapa Tabuleiros Costeiros, Documentos, 221).

Raes, D., Steduto, P., Hsiao, T.C., Fereres, E., 2009. AquaCrop—the FAO crop model to simulate yield response to water: II. Main algorithms and software description. Agron. J. 101, 438–447.

Rampazo, N.A.M., Picoli, M.C.A., Teixeira, A.H. de C., Cavaleiro, C.K.N., 2020. Water consumption modeling by coupling MODIS images and agrometeorological data for sugarcane crops. Sugar Tech 23, 524–535.

Raupasch, M.R., 2001. Combination theory and equilibrium evaporation. Q. J. R. Meteorol. Soc. 127, 1149–1181.

Ribeiro, M.C., Metzger, J.P., Martensen, A.C., Ponzoni, F.J., Hirota, M.M., 2009. The Brazilian Atlantic Forest: how much is left, and how is the remaining forest distributed? Implications for conservation. Biol. Conserv. 142, 1141–1153.

Rodrigues, A.F., Mello, C.R. de, Terra, M.C.N.S., Beskow, S., 2021. Water balance of an Atlantic Forest remnant under a prolonged drought period. Cienc. E Agrotecnol 45, e008421.

Safre, A.L.S., Nassar, A., Torres-Rua, A., Aboutalebi, M., Saad, J.C.C., Manzione, R.L., Teixeira, A.H. de C., Prueger, J.H., McKee, L.G., Alfieri, J.G., Hipps, L.E., Nieto, H., White, W.A., Alsina, M., del, M., Sanchez, L., Kustas, W.P., Dokoozlian, N., Gao, F., Anderson, M.C., 2022. Performance of Sentinel-2 SAFER ET model for daily and seasonal estimation of grapevine water consumption. Irrigat. Sci. 40, 635–654.

Sandre Osorio, I., Murilo, D., 2008. UNESCO Office Montevideo and Regional Bureau for Science in Latin America and the Caribbean Agua y Diversidad Cultural en México. IMTA: Cuernavaca, Mexico, p. 246p.

Santos, J.E.O., Cunha, F.F., Filgueiras, R., Silva, G.H., Teixeira, A.H. de C., Silva, F.C.S., Sediyama, G.C., 2020. Performance of SAFER evapotranspiration using missing meteorological data. Agric. Water Manag. 233, 1–8.

Seneviratne, S.I., Corti, T., Davin, E.L., Hirschi, M., Jaeger, E.B., Lehner, I., Orlowsky, B., Teuling, A.J., 2010. Investigating soil moisture–climate interactions in a changing climate: a review. Earth Sci. Rev. 99, 125–161.

Silva, P.F. da, Lima, J.R. de S., Antonino, A.C.D., Souza, R., Souza, E.S., de Silva, J.R.I., Alves, E.M., 2017. Seasonal patterns of carbon dioxide, water, and energy fluxes over the Caatinga and grassland in the semi-arid region of Brazil. J. Arid Environ. 147, 71–82.

Silva, C.O.F., Teixeira, A.H. de C., Manzione, R.L., 2019. An R package for spatial modelling of energy balance and actual evapotranspiration using satellite images and agrometeorological data. Environ. Model. Software 120, 104497.

Silva, J.L.B. da, Moura, G.B. de A., Silva, M.V. da, Oliveira-Júnior, J.F., de Jardim, A.M.R.F., Refati, D.C., Lima, R.C.C., Carvalho, A.A. de, Ferreira, M.B., Brito, J.I.B.B., Guedesf, R.V.S., Lopes, P.M.O., Nobrega, R.S., Pandorfi, H., Bezerra, A.C., Batista, P.H.D., Jesus, F.L.F., Sanches, A.C., Santos, R.C., 2023. Environmental degradation of vegetation cover and water bodies in the semiarid region of the Brazilian Northeast via cloud geoprocessing techniques applied to orbital data. J. South Am. Earth Sci. 121, 104164.

Sumner, D.M., Jacobs, J., 2005. Utility of penman-Monteith, Priestley-Taylor, reference evapotranspiration, and pan evaporation methods to estimate pasture evapotranspiration. J. Hydrol. 308, 81–104.

Teixeira, AH. de C., 2010. Determining regional actual evapotranspiration of irrigated and natural vegetation in the São Francisco River basin (Brazil) using remote sensing and Penman-Monteith equation. Rem. Sens. 2, 1287–1319.

Teixeira, A.H. de C., Bastiaanssen, W.G.M., Ahmad, M.D., Moura, M.S.B., Bos, M.G., 2008. Analysis of energy fluxes and vegetation-atmosphere parameters in irrigated and natural ecosystems of semi-arid Brazil. J. Hydrol. 362, 110–127.

Teixeira, A.H. de C., Scherer-Warren, M., Hernandez, F.B.T., Andrade, R.G., Leivas, J.F., 2013. Large-scale water productivity assessments with MODIS Images in a changing Semi-Arid environment: a Brazilian case study. Rem. Sens. 5, 5783–5804.

Teixeira, A.H. de C., Leivas, J.F., Silva, G.B., 2017. Drought assessments by coupling Moderate Resolution Imaging Spetroradiometer images and weather data: a case study in the Minas Gerais state, Brazil. In: Petropoulos, G.P., Islam, T. (Eds.), Remote Sensing of Hydrometeorological Hazards. 1 ed., Taylor & Francis, Boca Raton-FL, pp. 53–68.

Teixeira, A.H. de C., Simão, F.R., Leivas, J.F., Gomide, R.L., Reis, J.B.R.S., Kobayashi, M.K., Oliveira, F.G., 2018. Water productivity modeling by remote sensing in the semiarid region of Minas Gerais state, Brazil. In: Yuksel, I., I, Arman, H. (Eds.), Arid Environments and Sustainability. InTech, London, pp. 94–108.

Teixeira, A.H. de C., Takemura, C.M., Leivas, J.F., Pacheco, E.P., Silva, G.B., Garçon, E.A.M., 2020. Water productivity monitoring by using geotechnological tools in contrasting social and environmental conditions: applications in the São Francisco River basin, Brazil. Remote Sens. Appl.: Soc. Environ. 18, 1–9.

Teixeira, A.H. de C., Leivas, J.F., Pacheco, E.P., Garçon, E.A.M., Takemura, C.M., 2021. Biophysical characterization and monitoring large-Scale water and vegetation anomalies by remote sensing in the agricultural growing areas of the Brazilian semi-arid region. In: Pandey, P.C., Sharma, L.K. (Eds.), Advances in Remote Sensing for Natural Resource Monitoring. 1 ed., Wiley Online Library 1, New Jersey, pp. 94–109.

Vanella, D., Ramírez-Cuesta, J.M., Intrigliolo, D.S., Consoli, S., 2019. Combining electrical resistivity tomography and satellite images for improving evapotranspiration estimates of Citrus orchards. Rem. Sens. 11 (4), 373.

Venâncio, L.P., Mantovani, E.C., Amaral, C.H. do, Neale, C.M.U., Filgueiras, R., Gonçalves, I.Z., Cunha, F.F. da, 2021. Evapotranspiration mapping of commercial corn fields in Brazil using SAFER algorithm. Sci. Agric. 78, 1–12.

Villalobos, F.J., Testi, L., Orgaz, F., García-Tejera, O., Lopez-Bernal, A., González-Dugo, M.V., Ballester-Lurbe, C., Castel, J.R., Alarcón-Cabañero, J.J., Nicolás-Nicolás, E., 2013. Modelling canopy conductance and transpiration of fruit trees in Mediterranean areas: a simplified approach. Agric. For. Meteorol. 171, 93–103.

Wagle, P., Bhattarai, N., Gowda, P.H., Kakani, V.G., 2017. Performance of five surface energy balance models for estimating daily evapotranspiration in high biomass sorghum. ISPRS J. Photogrammetry Remote Sens. 128, 192–203.

Yang, Y., Guan, H., Batelaan, O., McVicar, T.R., Long, D., Piao, S., Liang, W., Liu, B., Jin, Z., Simmons, C.T., 2016. Contrasting responses of water use efficiency to drought across global terrestrial ecosystems. Sci. Rep. 6, 1–8.

Zhang, F., Zhou, G., Wang, Y., Yan, F., Christer Nilsson, C., 2012. Evapotranspiration and crop coefficient for a temperate desert steppe ecosystem using eddy covariance in Inner Mongolia, China. Hydrol. Process. 26, 379–386.

Zhang, X., Zhang, B., 2019. The responses of natural vegetation dynamics to drought during the growing season across China. J. Hydrol. 574, 706–714.

Zhou, L., Zhou, G., 2009. Measurement and modeling of evapotranspiration over a reed (Phragmites australis) marsh in Northeast China. J. Hydrol. 41–47. 372.